Proc. of the 9th Intl. Conf. of Asian Society for Precision Engg. and Nanotechnology (ASPEN 2022)
15–18 November 2022, Singapore. Edited by Nai Mui Ling Sharon and A. Senthil Kumar
doi://10.3850/978-981-18-6021-8_OR-02-0284

Hybrid electromagnetic actuator with a dual rotor configuration

Jonathan Hey[1#], Akash Singh[1]

1 Adaptive Robotics and Mechatronics Group, Singapore Institute of Manufacturing Technology, 2 Fusionopolis Way, 138634, Singapore
Corresponding Author / Email: Jonathan-hey@simtech.a-star.edu.sg, TEL: +65 6510 1365

KEYWORDS: Actuation, Electromagnetics, Mobile robots

A mobile robot is required to operate in various environment depending on the application needs. For instance, when working outdoors, the mobile robot may need to navigate rocky terrain; indoors, it may need to overcome challenges like scaling stairs. It is important that the mobile robot has the versatility to operate in an unstructured environment to make it truly useful. The key enabler of such versatile operation lies in the locomotion mechanism of the mobile robot. Recent research activities in this area have seen the development of transformable, deployable and shape changing wheels, giving the mobile robot some mechanical advantage to overcome obstacles or rough terrain. However, one of the key limitations in implementing of such transformable wheels is the actuator or the motor drive unit. For example, when a robot with transformable wheels switches from wheeled to legged motion, the torque demand on the motor increases significantly. Currently, most commercially available electric motors that are available commercially are optimized for a single purpose. In this paper, a dual rotor hybrid electromagnetic actuator that is designed for both high speed wheeled locomotion as well as high torque legged locomotion at lower speed is presented together with a simulation of its electromechanical characteristics through a numerical model of the actuator.

NOMENCLATURE

A	Vector potential [Wb/m]
B	Magnetic flux density [T]
F	Force [N]
H	Magnetic field strength [A/m]
J	Current density [A/m^2]
M	Magnetization [A/m]
Greek letters	
μ_r	Relative Permeability
μ_0	Permeability of free space [H/m]
λ	Rotor segment thickness [mm]
σ	Stress tensor [N/m^2]
τ	Torque [Nm]
χ	Susceptibility
ω	Angular speed [rad/s]
Φ	Magnetic flux (Wb)

1. Introduction

There is no single actuator available which is suited for both high speed wheeled locomotion as well as high torque legged locomotion at lower speed [1]. There has been some reports of electromagnetic actuator with multiple rotors with different magnetic pole arrangements that can produce higher levels of torque over a larger range of speed [2]. At near zero or low speeds, the first set of permanent magnet assembly (with high number of magnetic poles) will be activated to allow for larger torque production at this near stationary condition [3]. Once initial motion is attained, a secondary set of permanent magnet assembly (with less magnetic poles) is activated to achieve the higher speed motion [4].

The dual rotor configuration presented in this paper would overcome the limitations of the low torque production at low speeds in a conventional electric motor. The hybrid actuator is capable of producing high torque outputs across a much larger range of speed due to the innovations made to the rotor design and configuration. An electromagnetic analysis is conducted to estimate the output characteristics of the dual rotor hybrid actuator. The simulated electromechanical characteristics is presented and a qualitative comparison is made against other more conventional electric motors.

2. Mathematical modelling

In this section, the analysis of the magnetic fields in the region surrounding the permanent magnetic and thermomagnetic material is outlined and described. A magnetostatics analysis is conducted in this design analysis. Firstly, Gauss law states that the magnetic flux (B) across any surface enclosing a volume is equal to zero or $\nabla \cdot B = 0$. Secondly, the Ampere-Maxwell law states that the curl of the magnetic field (H) at any point in space is equal to the current density, $J = \nabla \times H$. Assuming that there are no other magnetic material present in this region, then the flux density is proportional to the field intensity $(B = \mu_0 H)$ which leads to the following expression:

$$\nabla \times B = \mu_0 J \quad (4)$$

A vector potential A can be defined which satisfies the following condition, $B = \nabla \times A$. Using this definition of the vector potential, the magnetostatic equations can be expressed in terms of the vector

potential as such:

$$\nabla \times (\nabla \times A) = \mu_0 J \quad (5)$$

Finally, assuming that the coulomb gauge condition is met, then the following expression of the magnetostatics is obtained:

$$\nabla^2 A = -\mu_0 J \quad (6)$$

Equation (6) completely describes the magnetic field in free space where the only magnetic source is a steady current with density equal to J [5].

In the regions where there are permanent magnetic materials present, the constitutive relationship, $B = \mu_0(H + M)$, is true whereby M is the magnetization field vector contributed by the magnetic material which can be expressed as an equivalent current density ($J_M = \nabla \times M$). For linear and isotropic magnetic materials, the magnetization of the material is proportional to the magnetic field intensity such that $M = \chi H$ whereby χ is the magnetic susceptibility of the material. This gives rise to the following form of the constitutive relationship, $B = \mu_0(1 + \chi)H$, which is expressed in terms of relative permeability of the material, $\mu_r = (1 + \chi)$.

With the relative permeability defined, the magnetostatic equation described in (6) can be further generalized to include the effects of the material by the following expression:

$$\nabla \times H = J_M$$

$$\nabla \times \left(\frac{1}{\mu_0 \mu_r} B\right) = J_M \quad (7)$$

Using the earlier definition of the vector potential, the original magnetostatic formulation is expressed in terms of the vector potential and the relative permeability of the magnetic material:

$$\nabla \times \left(\frac{1}{\mu_0 \mu_r} \nabla \times A\right) = J_M \quad (8)$$

Equation (8) describes the magnetic field in permanent magnetic materials and it should be used only in regions where there are linear and isotropic permanent magnetic materials present. The voltage induced in the material is evaluated through faraday's law of electromagnetic induction which is described mathematically by (9).

$$\mathrm{E} = \frac{d\Phi}{dt} \quad (9)$$

where Φ is the magnetic flux that is bounded by a closed loop traced out by the path L or the area S that is enclosed by this path which is defined here by (10):

$$\oint_L \mathrm{A}.d\mathrm{L} = \int \int_s \nabla \times \mathrm{A} \cdot d\mathrm{S} = \Phi \quad (10)$$

The next step of the design analysis requires the evaluation of the magnetic forces that is acting on the thermomagnetic material in order to produce the torque and rotation. The total magnetic force acting on a volume of magnetic material subjected to an external magnetic field with flux density B is given by this expression:

$$F = \frac{1}{\mu_0} \iiint dV\, (\nabla \times B) \times B \quad (11)$$

This volumetric force can be expanded in terms of the components of flux acting on the bounding surface S that encloses this volume. Expressing this force in terms of the surface flux density gives rise to the following formulation in terms of the stress tensor (σ) [6]

$$F = \oint_s n \cdot \sigma \, dS \quad (12)$$

where n is the vector normal to the surface S and the stress tensor is defined as such:

$$\sigma = \frac{1}{\mu_0}\left[BB^T - \frac{1}{2} B \cdot B\right] \quad (13)$$

The torque that is generated on this volume is then evaluated by integrating the cross product of this force and the moment arm along the entire surface of the bounded volume.

$$\tau = \frac{1}{\mu_0} \oint_s (r - r_0) \times n \cdot \sigma \, dS$$
$$= \frac{1}{\mu_0} \oint (r - r_0) \times n \cdot \left[BB^T - \frac{1}{2} B \cdot B\right] dS \quad (14)$$

where $(r - r_0)$ is normal distance from the axis of rotation. Further details of the magnetic analysis method is found in [7].

3. Dual rotor motor design and configuration

The design of the dual rotor hybrid electromagnetic actuator is illustrated by the CAD model shown in Figure 1. The actuator has a stationary winding assembly sandwiched between an inner and outer rotor. The two rotors are mechanically decoupled and free to rotate independently at different speeds. The permanent magnets are located on the rotors while the windings are installed onto the stator. Figure 1(a) shows the arrangement of the stator which is attached to the mounting (in green) that acts as the fixed support for the stator. The inner rotor (in dark brown) in Figure 1(b) is attached to an output flange that acts like an output shaft for the inner rotor. The output lever transfers mechanical torque from the outer rotor (in beige). Figure 1(c) shows the unique design of the stator which has two sets of windings with slightly different configurations. The outer winding has three phases of concentrated windings inserted into a total of 18 slots while the inner winding has only two phases concentrated in only 8 slots.

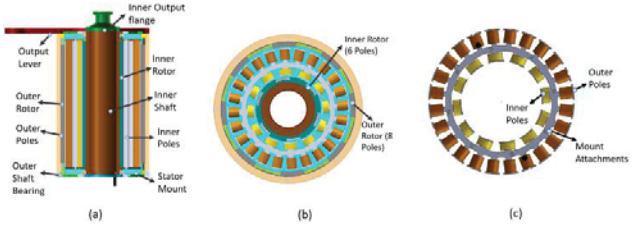

Figure 1: The above CAD depictions shows following a) the cross section view of the dual stator-rotor actuator, b) Cross section view of poles of the inner and outer rotor and c) the front view of the stator slot arrangements.

There are a total of 3 magnetic pole pairs in the inner rotor while the outer rotor has a total of 4 magnetic pole pairs. The outer rotor has a diameter of 0.2m while the inner rotor has a diameter of 0.1m with a length of 0.3m. The slots are about 0.01m in depth and 0.01m wide. Wires with a diameter of 1 mm is used to construct the windings with a total of about 100 series turns in each phase of the winding. This particular configuration of magnetic poles on the rotor and windings in the stator leads to a higher torque output at the outer rotor at lower speeds. Higher speeds can be achieved by the inner rotor at lower voltages due to the lower air gap flux. Also, the smaller diameter of the inner rotor does limit the torque output but it would allow it to spin up to a higher speed. The list of motor parameters are given in Table 1.

Table 1: List of key motor parameters

Dimensions		**Rotor configurations**	
Inner rotor diameter	0.1m	Outer poles	8
Outer rotor diameter	0.2m	Inner poles	6
Air gap	2.5mm	Stator configuration	
Stator slot height	0.01m	Outer slots	24
Stator slot width	0.01m	Inner slots	12
Winding configuration			
Outer winding phases	3	Inner winding phases	2

**Concentrated winding with 100 of series turns of 1mm diameter wire*

3. Simulation results

The mathematical model described earlier in section 2 is implemented with a finite element method to determine the input-output characteristics of the dual rotor actuator. Figure 2 shows the magnetic field lines generated by the permanents magnets and windings. The simulation shows that there are some cross linkages of magnetic flux between the inner and outer rotors. This would affect the 'smoothness'of the torque that can be produced. Also, there are some areas in the stator where the magnetic field lines appears to be

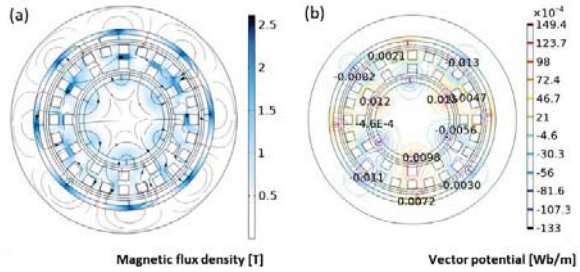

limited by the magnetic saturation of the material. These are some of the possible limitations of the dual rotor configuration that might reduced the effectiveness of the actuator.

Figure 2: (a) Contour plots of the magnetic flux density and (b) contour lines of the magnetic vector potential

With data generated from the numerical model, the electromechanical characteristics of the actuator is determined by evaluating the voltage constant [V_{rms}/RPM] and torque constant [Nm/A_{rms}] which are defined in (15) and (16) respectively.

$$K_e = \frac{V}{\omega} \quad (15)$$

$$K_t = \frac{\tau}{I} \quad (16)$$

The induced voltage (V) in the stator windings at a given rotational speed is determined from (9). On the other hand, the electromagnetic torque that is generated when a current (I) is supplied to the stator windings is evaluated using (14).

Figure 3 shows one period of the phase voltage induced in the outer and inner windings plotted against time. The outer phase windings are denoted by A, B, C while the inner phase windings are U, V. The voltage waveform is generated at a constant rotation speed of 1000RPM. The rotation speed is related to the fundamental frequency (f) of the phase voltage according to this relationship, $f = p\omega/120$, where ω is the rotation speed in RPM and p is the number of poles. This gives rise to a slight difference in the fundamental frequency of the inner and outer phase voltages which is reflected by the shorter time period for each cycle. The voltage

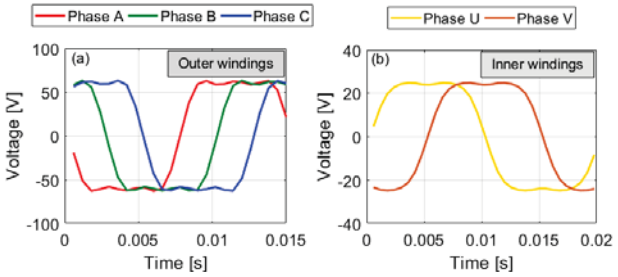

constant is evaluated using (15) by taking the RMS value of the phase voltages. The model estimates a voltage constant of about 55V/kRPM for the outer rotor and 14V/kRPM for the outer rotor.

Figure 3: Voltage induced in the outer and inner windings at 1000RPM

The voltage constant dictates the maximum achievable speed of the motor at the limits of the supplied voltage. A lower voltage constant would mean that it can achieve a higher speed at lower voltages. This indicates that, when the same voltage is supplied, the inner rotor can spin faster than the outside rotor. Assuming that the motor driver is able to supply a RMS voltage of up to 60V, then the inner rotor is able to rotate at speeds of up to 4300RPM while the outer rotor reaches a top speed of only 1100RPM assuming no load conditions. This makes the dual rotor motor suited for a wider range of operating speed depending on which rotor is being engaged.

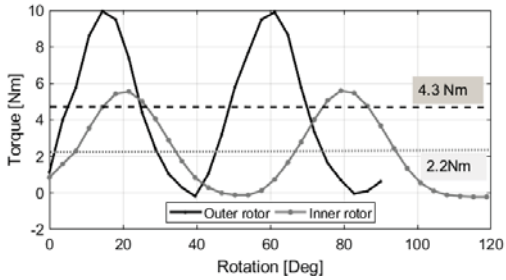

Figure 4: Torque generated by the outer and inner rotor at various rotation angle

Figure 4 shows the torque produced by the outer and inner rotor when a RMS current of 1A is supplied to the windings. The fluctuation in the torque is observed due to the concentrated windings used in this analysis. The ripples in the torque can be further minimized by distributing the windings and also shaping the slots and magnets to minimize the changes in the magnetic reluctance at different angles of the rotation. The averaged value of torque is plotted in the some graph in dashed lines. The outer rotor produces a higher level of torque on average compared to the inner rotor. The higher torque is achieved with the higher number of poles and also larger diameter of the rotor.

4. Conclusions

The magnetic analysis conducted in this work and the simulation results shows that the dual rotor hybrid actuator is suitable for both legged and wheel locomotion action. The combination of the high torque and lower nominal speed on the outer rotor makes it more suited for legged locomotion. On the other hand, the higher nominal speed achieved by the inner rotor is useful for driving the wheels though the torque generated is lower than the outer rotor. Combining the two rotors into one device would help to reduce the overall weight of the device. This would result in weight reductions when the dual rotor hybrid actuator is used in the final application and mounted on a mobile robot. This would help increase the payload or enhance the performance of the mobile robotic system.

REFERENCES

[1] C. Nie, X. Pacheco Corcho, and M. Spenko, "Robots on the move: Versatility and complexity in mobile robot locomotion," *IEEE Robot. Autom. Mag.*, vol. 20, no. 4, pp. 72–82, 2013, doi: 10.1109/MRA.2013.2248310.

[2] R. Qu and T. A. Lipo, "Dual-rotor, radial-flux, toroidally-wound, permanent-magnet machines," *Conf. Rec. - IAS Annu. Meet. (IEEE Ind. Appl. Soc.*, vol. 2, pp. 1281–1288, 2002, doi: 10.1109/IAS.2002.1042723.

[3] A. Dalal and P. Kumar, "Design, Prototyping, and Testing of

a Dual-Rotor Motor for Electric Vehicle Application," *IEEE Trans. Ind. Electron.*, vol. 65, no. 9, pp. 7185–7192, 2018, doi: 10.1109/TIE.2018.2795586.

[4] Y. H. Yeh, M. F. Hsieh, and D. G. Dorrell, "Different arrangements for dual-rotor dual-output radial-flux motors," *IEEE Trans. Ind. Appl.*, vol. 48, no. 2, pp. 612–622, 2012, doi: 10.1109/TIA.2011.2180495.

[5] P. P. Silvester and R. L. Ferrari, "Electromagnetics of finite elements," in *Finite Elements for Electrical Engineers*, 2012, pp. 68–125.

[6] S. J. Salon, "Calculation of Force and Torque," in *Finite Element Analysis of Electrical Machines*, New York, NY: Springer US, 1995, pp. 97–123.

[7] J. Hey, T. Jun Liang, and T. Zhi Hao, "An evaluation of thermomagnetic motors for heat energy harvesting," in Advanced Intelligent Mechatronics (AIM) conference, 15-17 July, 2022.